Polymerization kinetics of ADP- and ADP-P_i-actin determined by fluorescence microscopy

Ikuko Fujiwara*, Dimitrios Vavylonis*[†§], and Thomas D. Pollard*[‡¶]

Departments of *Molecular, Cellular, and Developmental Biology and Departments of [‡]Cell Biology and Molecular Biophysics and Biochemistry, Yale University, New Haven, CT 06520-8103; and [†]Department of Chemical Engineering, Columbia University, New York, NY 10027

Contributed by Thomas D. Pollard, March 23, 2007 (sent for review December 19, 2006)

We used fluorescence microscopy to determine how polymerization of Mg-ADP-actin depends on the concentration of phosphate. From the dependence of the elongation rate on the actin concentration and direct observations of depolymerizing filaments, we measured the polymerization rate constants of ADP-actin and ADP-P_i-actin. Saturating phosphate reduces the critical concentration for polymerization of Mg-ADP-actin from 1.8 to 0.06 μM almost entirely by reducing the dissociation rate constants at both ends. Saturating phosphate increases the barbed end association rate constant of Mg-ADP-actin 15%, but this value is still threefold less than that of ATP-actin. Thus, ATP hydrolysis without phosphate dissociation must change the conformation of polymerized actin. Analysis of depolymerization experiments in the presence of phosphate suggests that phosphate dissociation near the terminal subunits is much faster than in the interior. Remarkably, 10 times more phosphate is required to slow the depolymerization of the pointed end than the barbed end, suggesting a weak affinity of phosphate near the pointed end. Our observations of single actin filaments provide clues about the origins of the difference in the critical concentration at the two ends of actin filaments in the presence of ATP.

filaments | rate constant | treadmilling

A full understanding of actin dynamics in cells will require a complete set of kinetic and equilibrium constants for the polymerization and depolymerization reactions for the three different nucleotide states of actin monomers and polymers, which can bind ATP, ADP-P_i (ADP with inorganic phosphate [P_i] bound noncovalently in the γ-phosphate position), or ADP. Each of these species can bind and dissociate at both the fast growing barbed end and the slow growing pointed end of a filament. Monomeric actin hydrolyzes ATP very slowly (1), but polymerization changes the conformation of the subunits so that they hydrolyze ATP irreversibly (2) at 0.3 s^{-1} (3), assuming hydrolysis is random. The γ-phosphate dissociates slowly from the ADP-P_i intermediate with a half time of ≈350 s (4). The reaction is reversible, but the affinity of polymerized ADP-actin for inorganic phosphate is low, with a K_d in the millimolar range (5). Electron microscopy (6, 7) and limited proteolysis (8) indicate that P_i dissociation is coupled to a conformation change in the actin filament.

As a result of ATP hydrolysis, single actin filaments at steady state add fresh ATP-subunits at the barbed end balanced by dissociation of ADP-actin at the pointed end in a process known as treadmilling (9–12). Treadmilling in a medium containing ATP depends on hydrolysis of ATP bound to polymerized subunits and P_i dissociation coupled to differences in the rate constants for subunit association and dissociation at the two ends (9, 13). The critical concentrations of ATP-actin and ADP-P_i-actin are similar (14, 15), but some of the kinetic parameters required to model the steady state behavior of actin (16) were unknown, such as the association and dissociation rate constants for ADP-P_i-actin at both ends and for P_i binding ADP-actin monomers. The turnover of actin filaments in cells (17, 18) is much faster than expected from the treadmilling of filaments of purified actin.

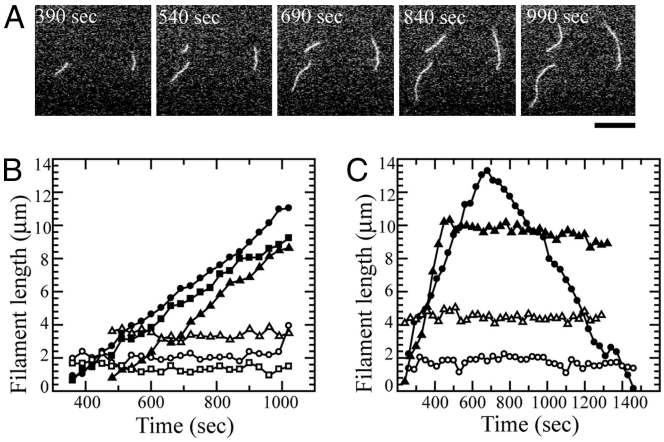

Fig. 1. Polymerization of Mg-ADP-actin SI Movies 1 and 2. Conditions were as follows: 50 mM KCl/1 mM $MgCl_2$/1 mM EGTA/10 mM imidazole, pH 7.0/100 mM DTT/0.2 mM ADP/15 mM glucose/20 μg ml^{-1} catalase/100 μg ml^{-1} glucose oxidase/0.5% methylcellulose at room temperature. (*A*) Time series of fluorescence micrographs showing the elongation of filaments by 3 μM Mg-ADP-actin 30% labeled with Alexa green. (Scale bar, 10 μm.) (*B*) Time course of elongation of three sample filaments by 3 μM ADP-actin. Filled symbols, barbed end; open symbols, pointed ends. Average elongation rates from linear fitting of 17 actin filaments under these conditions were 5.2 ± 0.1 s^{-1} at the barbed and 0.14 ± 0.04 s^{-1} at the pointed end. (*C*) Time course of depolymerization of sample filaments polymerized from 5 μM ADP-actin. Circles, polymerized and then washed with polymerization buffer containing 50 mM KCl and no actin at 620 s; triangles, polymerized and then washed with polymerization buffer containing 20 mM P_i and no actin at 440 s. Filled symbols, barbed end; open symbols, pointed ends.

We measured directly the association and dissociation rate constants of ADP-P_i-actin, using evanescent wave fluorescent microscopy. To reduce the rate of dissociation of Mg-ADP-actin, higher concentrations of P_i are required at pointed ends than at barbed ends. These parameters allowed us to propose a complete thermodynamic and kinetic description of the effects of ATP hydrolysis and γ-phosphate binding on actin polymerization.

Results

We used TIRF microscopy to measure the elongation and shortening of filaments of Mg-ADP-actin with 30% of the subunits labeled on lysine side chains with Alexa green. Our mass spectrometry showed that 1 to 2 lysines were labeled with Alexa green. This Alexa green-actin copolymerizes more readily with unlabeled actin

Author contributions: I.F., D.V., and T.D.P. designed research; I.F. and D.V. performed research; I.F., D.V., and T.D.P. analyzed data; and I.F., D.V., and T.D.P. wrote the paper.

The authors declare no conflict of interest.

[§]Present address: Department of Physics, Lehigh University, Bethlehem, PA 18015.

[¶]To whom correspondence should be addressed. E-mail: thomas.pollard@yale.edu.

This article contains supporting information online at www.pnas.org/cgi/content/full/0702510104/DC1.

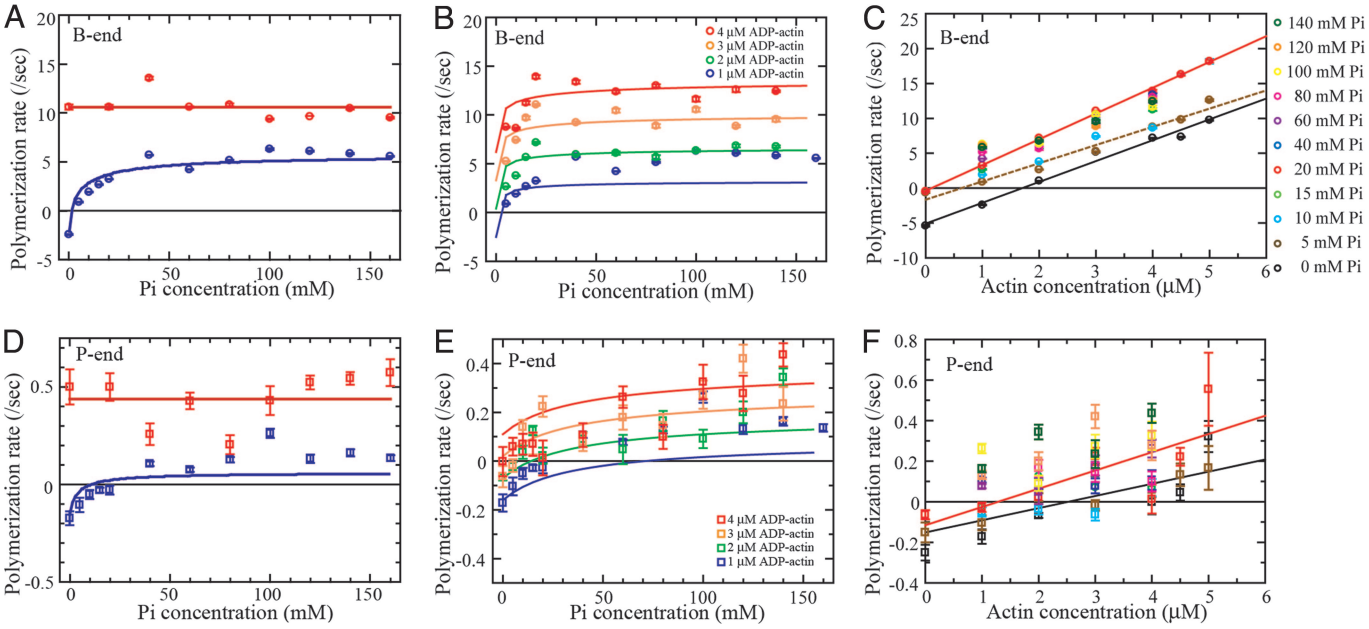

Fig. 2. Effect of P_i on elongation of actin filaments. Conditions were as in Fig. 1. To maintain constant ionic strength, the concentration of sulfate was varied such that the total concentration of P_i and sulfate was 160 mM, except the samples with <20 mM P_i, which did not have sulfate. (*A*) Dependence of the rate of elongation of barbed ends on the concentration of P_i. Red circles, 1 μM Mg-ATP-actin monomers; blue circles, 1 μM Mg-ADP-actin monomers. The curves are drawn through the data points. (*B*) Four different concentrations of Mg-ADP-actin monomers. The curves are global fits to the three highest ADP-actin concentrations (see *Discussion* and *SI Text*). (*C*) Barbed end elongation rate as a function of the concentration of Mg-ADP-actin monomers over a range of P_i concentrations. Black line and circles, 0 mM; broken line and brown circles, 5 mM; red line and circles, 20 mM; other P_i concentrations are defined by symbols on the graph. Error bars are ±1 standard deviation of the mean rates. The lines intersect the *x* axis at the critical concentrations. (*D*) Dependence of the rate of pointed end elongation on the concentration of P_i. Red squares, 1 μM Mg-ATP-actin; blue squares, 1 μM Mg-ADP-actin. (*E*) Dependence of the rate of pointed end elongation by four concentrations of Mg-ADP-actin monomers on P_i concentration. The curves are global fits to the three highest ADP-actin concentrations (see *Discussion*). (*F*) As in *C*, for the pointed end.

(19) than with actin labeled on cysteine-374 with rhodamine (20) or Oregon green (12), and the fluorescence of Alexa green-ADP-actin filaments was more intense. We used methylcellulose to suppress lateral Brownian movements of the actin filaments. A low density of NEM-myosin coating the glass kept actin filaments near the surface of the slide and created pivot points that we used as fiducial marks for measurements of contour lengths from the mark to each end of the filament (12).

Spontaneous nucleation of Mg-ADP-actin created filaments that grew steadily over time, much faster at barbed ends than at pointed ends (Fig. 1*A*). More filaments formed at higher concentrations of actin monomers. We measured the distances from a fiducial mark to both ends of each filament every 30 s (Fig. 1 *B* and *C*). We assumed that the faster growing end was the barbed end (11, 12). The steady rates of elongation over time verified that polymerization did not deplete the pool of actin monomers. We measured the average elongation rate of each filament from the slope of length vs. time and averaged 16–38 filaments for each condition [see supporting information (SI) Fig. 6 for details]. The measurement errors were similar at the two ends, so the error relative to the elongation rate was much smaller at the rapidly growing barbed ends.

Phosphate increased the elongation rate of Mg-ADP-actin at both ends of filaments (Fig. 2 *A–F*) but had no effect on elongation of either end by Mg-ATP-actin (Fig. 2 *A* and *D*). We used sulfate to maintain a constant ionic strength. We did not observe an effect of sulfate on polymerization at either end of the filaments in control experiments. The rate of elongation at barbed ends by Mg-ADP-actin increased with P_i concentration and plateaued at P_i concentrations over 40 mM at pH 7.0 (Fig. 2*B*), whereas elongation at pointed ends increased slowly over the whole range of P_i concentrations tested (Fig. 2 *D* and *E*). At high P_i concentrations the maximum rates of growth at both ends were less for ADP-actin than ATP-actin (Fig. 2 *A* and *D*).

We also observed dissociation of Mg-ADP-actin subunits directly from both ends of filaments with a range of P_i concentrations in the buffer (Fig. 3). After polymerizing 3 or 5 μM Mg-ADP-actin in the presence of P_i to identify the ends of each filament, we washed out free actin with polymerization buffer with the same concentration of P_i and observed steady rates of shortening at both ends (Fig. 1*C*). Dissociation of ADP-actin was faster at barbed ends than pointed ends (Fig. 3). We rarely observed severing events during depolymerization. With sampling every 30 s, we did not detect gradual changes in depolymerization rates following the washout of actin monomers.

Phosphate in the buffer slowed depolymerization at both ends, but ≈10 times more P_i was required for a half maximal effect at the pointed end than the barbed end (Fig. 3) (0.8 mM P_i at barbed end and 6.6 mM P_i at pointed end). We obtained similar results when ADP-actin was polymerized without P_i and then allowed to depolymerize in buffers containing P_i (data not shown).

We used plots of elongation rate vs. actin concentration to measure the rate constants for Mg-ADP-actin association (slopes) and dissociation (y-intercepts) without and with P_i (Fig. 2 *C* and *F*). The barbed end data fit well to straight lines, including the directly observed rates of depolymerization in the absence of free actin. Without P_i the association rate constant at barbed ends for Mg-ADP-actin is 2.9 $\mu M^{-1}s^{-1}$ and the dissociation rate constant is 5.4 s^{-1} by direct measurement and 4.9 s^{-1} by linear extrapolation. These dissociation rates are slightly less than the extrapolated value of 7.2 s^{-1} from EM experiments (10), but much larger than the dissociation rates of aged (22 min after polymerization) ATP-actin filaments (12).

With saturating P_i the barbed end association rate constant is 3.4 $\mu M^{-1}s^{-1}$ (Fig. 2*C*) and the dissociation rate constant is 0.2 ± 0.1

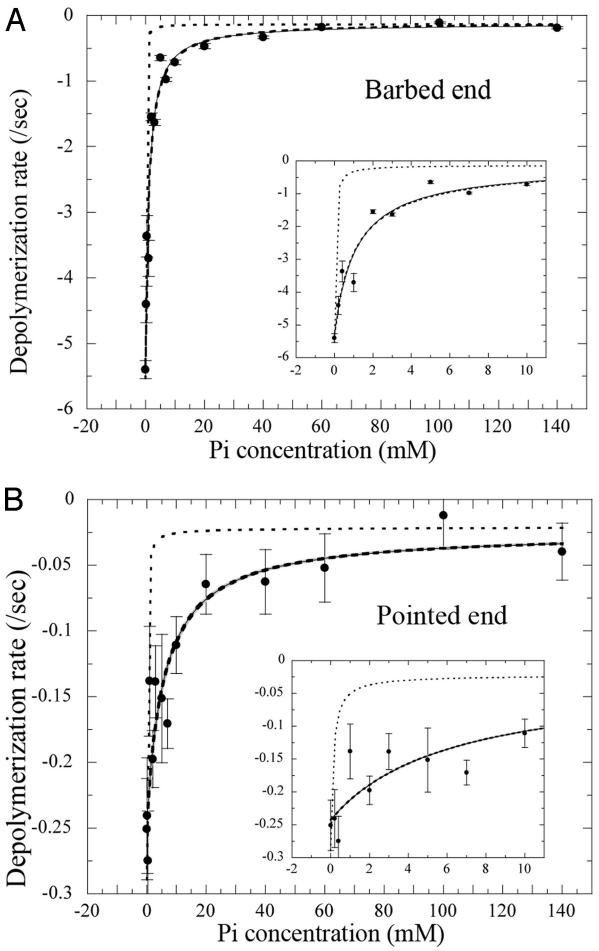

Fig. 3. Dependence of the dissociation of Mg-ADP-actin from the two ends of actin filaments on P_i. Conditions were as in Fig. 2 (the total ionic strength was standardized with sulfate). (*A*) Barbed end. The lines are fits to the data (see *SI Text* for all parameter values). Continuous line: rate of P_i dissociation from actin filaments is 0.003 s^{-1} and equilibrium P_i dissociation constant $K_d^{B2,3}$ = 50 mM. Dashed line: same as continuous line but the rate of P_i dissociation from terminal subunit is 20 s^{-1} and $K_d^{B2,3}$ = 1 mM. Dotted line: same as continuous line, but $K_d^{B2,3}$ = 1.5 mM. (*B*) Pointed end. Continuous line: uniform P_i dissociation rate 0.003 s^{-1}, dissociation equilibrium constant $K_d^{P2,3}$ = 60 mM. Dashed line: rate of P_i dissociation from terminal subunit is 20 s^{-1}, $K_d^{P2,3}$ = 6 mM. Gray line: same as dashed line, but the P_i dissociation equilibrium constant is 6 mM on the terminal subunit and 1.5 mM elsewhere. Dotted line: same as the continuous line, but $K_d^{P2,3}$ = 1.5 mM.

s^{-1} (Fig. 3*A*). Thus, P_i lowers the critical concentration >10-fold by reducing the dissociation rate constant at the barbed end by more than an order of magnitude along with a small increase in the association rate constant (Table 1).

Elongation at the pointed end is so slow that the values of the rate constants are less certain. Assuming that the critical concentrations for ADP-actin are the same at both ends (1.8 μM), and using the directly observed rate of dissociation of ADP-actin, 0.25 s^{-1} (Fig. 3*B*), we estimate that the ADP-actin association rate constant is 0.14 $\mu M^{-1}s^{-1}$, consistent with the value of 0.09 ± 0.03 $\mu M^{-1}s^{-1}$ measured from the slope of Fig. 2*F*. Phosphate reduces the dissociation rate constant ≈10-fold at the pointed end to ≈0.02 s^{-1} (Fig. 3*B*). Within experimental error P_i increased the association rate constant <50%, so the critical concentrations are approximately the same at both ends in saturating phosphate, as required.

Discussion

Our analysis of the association and dissociation rate constants for ADP-P_i-actin revealed two unexpected properties of actin. First, although Mg-ATP-actin and Mg-ADP-P_i-actin have similar critical concentrations, both the association and dissociation rate constants for Mg-ADP-P_i-actin are less than half those of Mg-ATP-actin at both ends of filaments (Fig. 2*A* and Table 1). Therefore, the assumption that Mg-ATP-actin and Mg-ADP-P_i-actin are identical kinetically is not true. This is evidence that ATP hydrolysis, even without dissociation of the γ-phosphate, changes the conformation of actin monomers and subunits in actin filaments in a way that alters their kinetic properties.

Second, the kinetics at the two ends of ADP-actin filaments have a different dependence on P_i concentration. This difference was most dramatic in depolymerization experiments where ten times more P_i is required for a half maximal effect on the pointed end (Fig. 3). As discussed below, this difference may be related to the difference in the critical concentrations at the two ends in ATP.

Our measurements of the rate constants for association and dissociation of ADP-P_i-actin allowed us to consider a full thermodynamic and kinetic analysis of actin polymerization and to explore why the two ends have different critical concentrations in the presence of ATP. For simplicity, we assume the existence of only one ADP-P_i-actin state, but we note that Combeau and Carlier (21) postulated two ADP-P_i-actin states when interpreting the effects of BeF_3 on actin assembly.

Thermodynamic and Kinetic Parameters of Actin Polymerization at the Barbed End. Here, we consider the rate and equilibrium constants for reactions at the barbed end (Fig. 4 and Table 1) and propose that P_i binding to the barbed end differs kinetically but not thermodynamically from the rest of the filament.

Reaction B1 (barbed end elongation by ATP-actin). These rate constants were measured by electron microscopy (10).

Reaction B2 (barbed end elongation by ADP-P_i-actin). We measured k_- directly in depolymerization experiments (Fig. 3) and k_+ from the elongation rate with saturating concentrations of P_i (Fig. 2*C*). The ratio of these rate constants (0.2 $s^{-1}/3.4\mu M^{-1}s^{-1}$ = 0.06 ± 0.03 μM) is statistically indistinguishable from the critical concentration of ATP-actin [0.12 ± 0.07 μM (10)], even though both rate constants differ for these two species.

Reaction B3 (barbed end elongation by ADP-actin). We reevaluated the rate and equilibrium constants for this reaction by direct microscopic observation (Figs. 2–3).

Reaction B1,2 (ATP hydrolysis by polymerized actin). The value of 0.3 s^{-1} (3) was calculated by assuming that ATP hydrolysis is a first order reaction with the same rate for all subunits of polymerized ATP-actin. We assume that the rate of ATP synthesis is near zero (5).

Reaction M1,2 (ATP hydrolysis by monomeric actin). Mg-ATP-actin monomers hydrolyze ATP at 0.000007 s^{-1} (1). We assume that the rate of ATP synthesis is near zero.

Reactions B2,3 and M2,3 (P_i binding to filaments and monomers). Direct measurements showed that P_i dissociates from ADP-P_i-actin filaments at 0.003 s^{-1} (22, 23) and equilibrium binding of $^{32}P_i$ to bulk filaments gave a $K_d^{B2,3}$ of 1.5 mM at pH 7.0 and 100 mM KCl (5). Thus, k_+ for P_i binding ADP-actin filaments is 2 $M^{-1}s^{-1}$. From microreversibility (13, 14, 21), $K_d^{B2,3} \times K_d^{B3} = K_d^{M2,3} \times K_d^{B2}$. The measured ratio of K_d^{B3} to K_d^{B2} is in the range of 20 to 60 depending on the difficult to measure value of ADP-P_i-actin dissociating from barbed ends. This constrains the dissociation equilibrium constant for P_i binding ADP-monomers ($K_d^{M2,3}$) to be in the range of 30 to 90 mM.

The dependence of ADP-actin dissociation rate on the concentration of P_i (Fig. 3*A*) provides additional constraints on the rate constants for P_i binding to the barbed end. If we use the measured affinity ($K_d^{B2,3}$ = 1.5 mM) and rate constants k_+ = 2 $M^{-1}s^{-1}$; k_- = 0.003 s^{-1}) for P_i binding ADP-actin filaments in an analytical expression derived in *SI Text*, the dependence of ADP-actin dissociation rate on P_i concentration (dotted line in Fig. 3*A*) deviates strongly from the data. This complication arises, because ADP-P_i- actin dissociates ≈25 times slower than

BIOPHYSICS

Table 1. Rate constants for reactions of Mg-actin with bound ATP, ADP-P_i, or ADP at barbed ends and pointed ends of actin filaments

Nucleotide state	End	k^+, $\mu M^{-1}s^{-1}$	k^-, s^{-1}	k^-/k^+, μM
Mg-ADP-actin*	Barbed	2.9 ± 0.21	5.4 ± 0.14†	1.8 ± 0.14
	Barbed		(4.9 ± 0.73)‡	(1.7 ± 0.27)§
	Pointed	0.09 ± 0.03	0.25 ± 0.04†	2.8 ± 1.0
Mg-ADP-P_i-actin*	Barbed	3.4 ± 0.08	0.2 ± 0.1†	0.06 ± 0.03
	Barbed		(0.2 ± 0.25)‡	(0.07 ± 0.07)§
	Pointed	0.11 ± 0.04	0.02 ± 0.02†	0.18 ± 0.30
Mg-ATP-actin¶	Barbed	11.6 ± 1.2	1.4 ± 0.8	0.12 ± 0.07
	Pointed	1.3 ± 0.2	0.8 ± 0.3	0.6 ± 0.17

*TIRF experimental data except for ATP-actin.
†Direct observation of dissociation process.
‡Dissociation rate estimated from *y*-intercepts in linear fit in Fig. 2.
§Ratios calculated using parameters labeled with ‡.
¶See ref. 10.

ADP-actin, so a small fraction of ADP-P_i-actin in the filament slows dissociation dramatically as observed for substoichiometric binding of BeF_3 (21). On the other hand, if P_i binds and dissociates rapidly (>2 s^{-1}) at the barbed end of actin filaments, the P_i concentration required to slow dissociation by half (≈1 mM; Fig. 3*A*) is approximately the same as the measured $K_d^{B2,3}$.

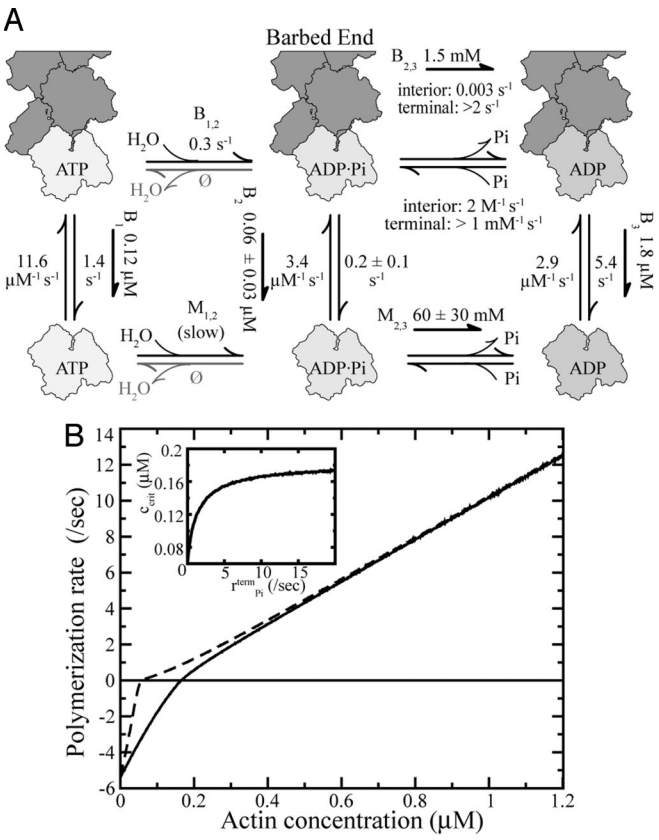

Fig. 4. Barbed end reactions. (*A*) Kinetic and thermodynamic parameters of barbed end polymerization including reactions of Mg-actin with bound ATP, ADP-P_i, or ADP. Numbers next to light arrows are rate constants and those next to bold arrows are ratios of rate constants (see *Discussion*). We indicate the standard deviations of the least certain values. The values for P_i binding to filaments apply to interior subunits. (*B*) Polymerization rate vs. ATP-actin concentration. Dashed line: theoretical calculations, using the values in *A*. Continuous line: as dashed line, but the rate constant for P_i dissociation from the terminal subunit is 20 s^{-1}. (*Inset*) ATP-actin critical concentration vs. rate of P_i dissociation from the terminal subunit.

This value is consistent with detailed balance and P_i binding to bulk filaments (5). This agreement suggests that the P_i association and dissociation rate constants are much larger at the barbed end but that the equilibrium constant is approximately the same as in the bulk of the filament.

Rapid P_i exchange near the barbed end is also consistent with the effect of P_i on elongation of barbed ends (Fig. 2*B*), the ability of 25 mM P_i to slow the depolymerization of ADP-actin filaments in <10 s (21), and our inability to detect transients in our washout experiments (Fig. 1*C*). Assuming fast P_i exchange, a global fit (see analytical expression in *SI Text*) to the elongation data gives $K_d^{B2,3}$ = 1.2 ± 0.5 mM and $K_d^{M2,3}$ = 35 ± 20 mM in agreement with binding measurements (5). If P_i exchange is as slow on the terminal subunit as in the interior of the filament, fitting the polymerization data in Fig. 2*B* with Monte Carlo simulations (see *SI Text*) requires a slightly higher P_i affinity, $K_d^{B2,3}$ = 0.5 ± 0.3 mM.

The mechanism with rapid P_i exchange on barbed ends accounts for the observed dependence of the barbed end elongation rate on the concentration of ATP-actin (Fig. 4*B*). We tested this mechanism by kinetic Monte Carlo simulations (24), using rate constants dependent on the nucleotide state of subunits associating or dissociating subunit at the end of the polymer (Fig. 4*A*) but independent of the nucleotide on adjacent subunits. We neglected the contributions of P_i, ADP- and ADP-P_i-actin association in these simulations. The calculated slope agrees with the experimental data, because those data were used to measure the rate constants. The calculated critical concentration depends on the rate of P_i dissociation from the terminal actin subunit and lies in the range 0.06 to 0.17 μM (Fig. 4*B Inset*). Numerous steady state and kinetic measurements give a barbed end critical concentration of 0.10 to 0.12 μM for ATP-actin, consistent with P_i exchanging faster at barbed ends than the bulk rate of dissociation.

The slope of elongation rate vs. [ATP-actin] is much steeper below than above the critical concentration because of rapid dissociation of ADP-actin below the critical concentration, where it occupies the barbed end with increasing frequency as the monomer concentration approaches zero (5, 24). If the reaction rates were strongly influenced by cooperative effects such as the influence of the nucleotide state of subunits near the end of the filaments, these plots would be curved (24). However, we note that given our assumptions, the dependence of elongation rate on [ATP-actin] is far less sensitive to the rate of P_i release than the rate of ADP-actin dissociation (Fig. 3*A*). For example, Stukalin and Kolomeisky (25) obtained similar plots of elongation rate vs. [ATP-actin], using much different assumptions of fast hydrolysis and vectorial P_i dissociation.

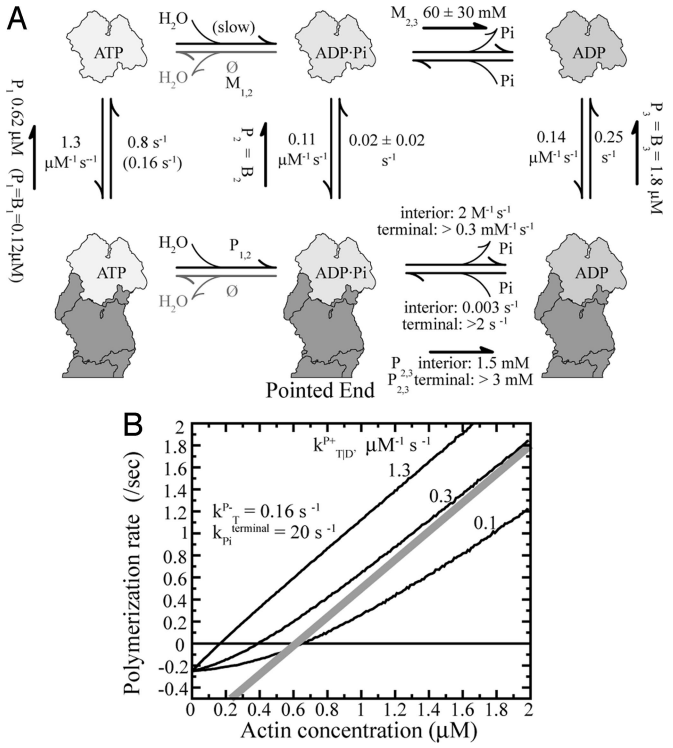

Fig. 5. Pointed end reactions. (*A*) Kinetic and thermodynamic parameters. Values in brackets for ATP-actin are consistent with detailed balance (see *Text*). (*B*) Pointed end polymerization rate vs. ATP-actin concentration for a range of association rate constants for ATP-actin binding terminal ADP-actin subunits, assuming that P_i dissociates from terminal subunits at $r_{Pi} = 20\ s^{-1}$, and using parameter values from *A* except for 0.16 s^{-1} for the ATP-actin dissociation rate constant. The gray line is the extrapolated linear fit from ref. 10 for ATP-actin.

Thermodynamic and Kinetic Parameters of Actin Polymerization at the Pointed End. The behavior of the pointed end is less clear than the barbed end for two reasons. First, measuring the rates of the very slow reactions is difficult. Second, long standing evidence suggests a simple mechanism, such as proposed in Fig. 4 for the barbed end, cannot account for the observations. Our evidence suggests that P_i binding at the pointed end differs both kinetically and thermodynamically from the rest of the filament (Fig. 5).

Reaction P1 (pointed end elongation by ATP-actin). The rate constants were measured from the linear dependence of the elongation rate on the concentration of ATP-actin (10, 12). The values of k_- and the critical concentration were calculated from positive growth rates and cannot be measured directly owing to hydrolysis of ATP bound to subunits in the filament.

Reaction P2 (pointed end elongation by ADP-P_i-actin). Within experimental error, the value of k_+ from the dependence of elongation rate on actin concentration is comparable with that of ADP-actin, and in saturating phosphate, it is $\approx 0.11\ \mu M^{-1}s^{-1}$. At high P_i concentration the dissociation rate plateaus at $\approx 0.02\ s^{-1}$.

Reaction P3 (pointed end elongation by ADP-actin). We assume that the equilibrium constant is the same as B3. We measured k_- ($0.25\ s^{-1}$) directly here (Fig. 3*B*). We calculate k_+ from ratio of measured k_- and assumed K_d^{B3}.

Reaction P1,2 (ATP hydrolysis by polymerized actin). Measurement of the ATP hydrolysis rate at the pointed end gave the same value as the barbed end (3).

Reaction P2,3 (P_i dissociation from pointed ends). Two lines of evidence show that the affinity of P_i for ADP-actin at the pointed end is lower than for ADP-actin subunits at the barbed end and throughout the filaments. (*i*) The concentration of P_i required to reduce the rate of ADP-actin dissociation by half is 6.6 mM at the pointed end, nearly 10-fold higher than at the barbed end (Fig. 3). Fitting this depolymerization data requires a very large $K_d^{P2,3}$ in the range of 20–80 mM, if one assumes uniformly slow P_i dissociation from filaments (see Fig. 3*B*). In contrast to the barbed end, even if we assume fast P_i dissociation from the terminal subunit, good fits still require $K_d^{P2,3}$ to be in the range of 3 to 9 mM (Fig. 3*B*). (*ii*) The elongation rates at the two ends differ in their dependence on the concentration of P_i. Assuming uniform P_i binding affinity and rapid equilibration on the terminal subunit, the fit to the elongation data in Fig. 2*E*, using the analytical expression in *SI Text*, gives $K_d^{P2,3} = 30 \pm 20$ mM, and $K_d^{M2,3} = 500 \pm 200$ mM.

These observations force us to consider that the terminal subunit at the pointed end has a lower affinity for P_i than the bulk of the filament as a result of cooperative interactions with neighboring subunits. This interesting possibility would, in turn, help to explain why the two ends have different critical concentrations in ATP as we discuss below.

Origin of the Differences in Critical Concentrations at the Two Ends in ATP. Some combination of ATP hydrolysis, P_i dissociation and conformational changes must account for the different critical concentrations at the two ends in buffer containing ATP (9, 13). Vavylonis *et al.* (24) argued that the difference in the critical concentrations is inconsistent with the assumption that hydrolysis and P_i dissociation occur uniformly along filaments, that ATP-actin is identical kinetically and thermodynamically to ADP-P_i-actin, and that rate constants depend only on the nucleotide bound to the associating or dissociating monomers. The three following experiments demand these complications be considered and suggests how kinetic cooperativity at the pointed end may be crucial.

1. The measured rate constants for ATP-actin at the two ends seem inconsistent with the principle of detailed balance, which requires that the ratio of the ATP-actin dissociation and association rate constants be the same at the two ends of the filament. Instead, the observed ratios are $K_d^{B1} = 0.12\ \mu M$ at the barbed end and $K_d^{P1} = 0.6\ \mu M$ at the pointed end, the same as the values of the critical concentrations obtained by other methods (5). Given $k_+ = 1.3\ \mu M^{-1}s^{-1}$ for ATP-actin association at the pointed end (10), k_- for ATP-actin at the pointed end would have to be $0.16\ s^{-1}$ to satisfy detailed balance ($K_d^{P1} = K_d^{B1}$), a much smaller rate than the extrapolated values of $0.9\ s^{-1}$ from TIRF microscopy experiments (12) and $0.8\ s^{-1}$ from EM (10). Thus, reactions other than ATP-actin dissociation probably contribute to the observed rate of dissociation from pointed ends with ATP-actin monomers in the bulk phase.
2. The observation that P_i decreases the critical concentration of the pointed end in the presence of ATP (2, 26) suggests that ADP-actin must be available to bind P_i at or near the pointed end. This ADP-P_i-actin, either by being the dissociating species or by indirect effects on the terminal subunit, would reduce the rate of dissociation at the pointed end and explain how P_i can decrease the pointed end critical concentration at steady state.
3. Our depolymerization experiments (Fig. 3) suggests that P_i dissociates rapidly from the terminal subunits at both barbed and pointed ends and that it has a weaker affinity for the terminal subunit at the pointed end than other parts of ADP-actin filaments. These differences must arise from interactions of subunits near the end of the filament. As described in *SI Text*, this leads us to consider the possibility that one or more rate constants depend on the nucleotide bound to actin subunits near the pointed end of the filament as suggested by Pantaloni *et al.* (27) to explain other aspects of actin elongation. Simple mechanisms respecting detailed balance as shown in Figs. 4*A* and 5*A* do not include reactions that account for such effects and no theory exists to describe their influence on the critical concentration.

Mechanisms with cooperative association kinetics and fast dissociation of P_i from the pointed end can explain different critical concentrations at the two ends with ATP in the buffer. Fig. 5*B* show how the elongation rate at the pointed end depends on the concentration of ATP-actin with the mechanisms in Fig. 5*A* modified in three different ways. First, for consistency with detailed balance, we assume the dissociation rate constant for ATP-actin at the pointed end k_T^{P-} is 0.16 s^{-1} rather than the apparent value of 0.8 s^{-1}. Second, we assume that P_i dissociates faster from pointed ends than from bulk filaments (a rate faster than $\approx$1 s^{-1} is required to obtain the effects shown in Fig. 5*B*). Third, we let the nucleotide bound to subunits near the end of the filament influence the association rate constant for ATP-actin.

We obtain a realistic value for the critical concentration at the pointed end if we assume that the rate constant for association of ATP-actin onto a pointed end with an ADP-actin terminal subunit, $k_{T|D}^{P+}$ is smaller than that onto an ATP-actin terminal subunit, $k_{T|T}^{P+}$, or onto ADP-P_i-actin, $k_{T|P}^{P+} = k_{T|T}^{P+}$. This assumption is consistent and in fact suggested by detailed balance constraints, assuming that the K_d describing the equilibrium between (*i*) ATP hydrolysis and P_i release and (*ii*) ATP synthesis is higher at the terminal subunit of the pointed end as compared with the bulk of the filament (analogous to the binding of P_i); see *SI Text*. Thus, under nonequilibrium conditions involving net hydrolysis, conversion of ATP into ADP at the terminal subunit slows association and increases the critical concentration. Note that in Fig. 5*B*, the elongation rate is linear for large actin concentrations as observed for a pure ATP-actin polymerization (10). However, the effective dissociation rate constant inferred from a linear extrapolation to zero actin (0.8 s^{-1}) is larger than the intrinsic ATP-actin dissociation rate of 0.16 s^{-1}. This effective dissociation rate constant is a composite number involving a combination of many rate constants, including the rates of association and hydrolysis, in addition to ATP-actin dissociation. The shape of the curves of Fig. 5*B* is consistent with prior experiments on pointed end elongation near the critical concentration using bulk assays (28–30).

Bindschadler *et al.* (16) simulated the dynamic behavior an actin filament 1 μm long at steady state with ATP, assuming that the rate constants depend only on the nucleotide bound to the associating or dissociating monomer. Because we suggest that rate constants may depend on neighbors, we were unable to use our new numbers in their model, which is available online.

Clearly, much more needs to be learned regarding the pointed end. Schemes beyond those outlined above are also conceivable [for example, involving vectorial hydrolysis (27)]. Although the experiments will be challenging, gaining more information about the details of ATP hydrolysis at both ends is important, because these reactions are likely to play a crucial role in the thermodynamics and kinetics of the actin cycle in cells (31).

Effect of Cytoplasmic Phosphate on the Assembly of ATP-Actin in Cells. If the concentration of P_i in nonmuscle cells is similar to the concentration of $\approx$5 mM in skeletal muscle (32), P_i will partially saturate the ADP-actin subunits in actin filaments and strongly suppress treadmilling by inhibiting dissociation of ADP-actin at both ends (Fig. 3). Partial saturation of filaments with P_i will also influence the ability of ADF/cofilins to bind and sever filaments (33).

Materials and Methods

Proteins. Actin was purified from rabbit skeletal muscle (34) and stored in buffer G (2 mM Tris·HCl, pH 8.0/0.2 mM ATP/1 mM NaN_3/0.1 mM $CaCl_2$/0.5 mM DTT). We labeled 9 mg of Ca-actin filaments in 4.5 ml of 100 mM KCl, 50 mM Pipes pH 6.8, 0.2 mM ATP, and 0.2 mM $CaCl_2$ with 1.5 mg of Alexa Fluor 488 carboxylic acid succinimidyl ester (Molecular Probes, Eugene, OR; catalog no. A20100) dissolved in dimethylformamide (DMF; Sigma, St. Louis, MO) over night at 4°C (19). Great care is required to prepare a homogeneous sample of Mg-ADP-actin. Incubation of Mg-ATP-actin with soluble hexokinase and glucose (35) works. Incubation with hexokinase immobilized on beads, which is adequate for preparing actin for nucleotide exchange experiments (36), does not remove all of the ATP and gives ambiguous results.

Experimental Conditions. Experiments were carried out in chambers constructed on 25 × 75 × 1 mm glass microscope slides (Chase Scientific Glass, Rockwood, TN) (12). These chambers were pretreated with 5 μl of 50 nM NEM-myosin and 200-nm-diameter red fluorescent beads (Molecular Probes) for focusing (12) and washed with 1% BSA. Actin was mixed with polymerization buffer in a test tube at room temperature and immediately transferred to the sample chamber. The samples consisted of 30% Alexa green-labeled actin in 50 mM KCl, 1 mM $MgCl_2$, 1 mM EGTA, 0.2 mM ADP, 10 mM imidazole·HCl pH 7.0, 100 mM DTT, and 0.5 (wt/vol)% methylcellulose for observing ADP-actin. Sodium sulfate was added to phosphate buffer to maintain a constant ionic strength.

Optical System. We observed single fluorescent actin filaments with prism-style total internal reflection fluorescence illumination from a 488-nm laser on an IX71 microscope (Olympus, Tokyo, Japan). Images were captured with 500 ms exposures of ORCA-ER camera (Hamamatsu Corporation, Hamamatsu, Japan) with a pixel size corresponding to 0.17 μm in the plane of the sample. Image J software was used to measure actin filament length (12).

We thank Jeffrey Kuhn and Rachel Mahaffy for their help; Enrique De La Cruz, Carl Frieden, and Jim McGrath for their thoughtful suggestions on the manuscript; and Ben O'Shaughnessy for discussions and support. This study was supported by a fellowship from the Japan Society for the Promotion of Science and National Institutes of Health Research Grant GM026338.

1. Rould MA, Wan Q, Joel PB, Lowey S, Trybus KM (2006) *J Biol Chem* 281:31909–31919.
2. Carlier MF, Pantaloni D, Evans JA, Lambooy PK, Korn ED, Webb MR (1988) *FEBS Lett* 235:211–214.
3. Blanchoin L, Pollard TD (2002) *Biochemistry* 41:597–602.
4. Carlier MF, Pantaloni D (1986) *Biochemistry* 25:7789–7792.
5. Carlier MF, Pantaloni D (1988) *J Biol Chem* 263:817–825.
6. Nonomura Y, Katayama E, Ebashi S (1975) *J Biochem* 78:1101–1104.
7. Belmont DL, Orlova A, Drubin GD, Egelman HE (1999) *Proc Natl Acad Sci USA* 96:29–34.
8. Muhlrad A, Pavlov D, Peyser YM, Reisler E (2006) *FEBS J* 273:1488–1496.
9. Wegner A (1976) *J Mol Biol* 108:139–150.
10. Pollard TD (1986) *J Cell Biol* 103:2747–2754.
11. Fujiwara I, Takahashi S, Tadakuma H, Funatsu T, Ishiwata S (2002) *Nat Cell Biol* 4:666–673.
12. Kuhn JR, Pollard TD (2005) *Biophys J* 88:1387–1402.
13. Hill TL (1987) *Linear Aggregation Theory in Cell Biology* (Springer, New York).
14. Wanger M, Wegner A (1987) *Biochim Biophys Acta* 914:105–113.
15. Rickard JE, Sheterline P (1986) *J Mol Biol* 191:273–280.
16. Bindschadler M, Osborn EA, Dewey CF, Jr, McGrath JL (2004) *Biophys J* 86:2720–2739.
17. Waterman-Storer C, Duey DY, Weber KL, Keech J, Cheney RE, Salmon ED, Bement WM (2000) *J Cell Biol* 150:361–376.
18. Watanabe N, Mitchison TJ (2002) *Science* 295:1083–1086.
19. Mahaffy RE, Pollard TD (2006) *Biophys J* 91:3519–3528.
20. Amann KJ, Pollard TD (2001) *Nat Cell Biol* 3:306–310.
21. Combeau C, Carlier MF (1988) *J Biol Chem* 263:17429–17436.
22. Blanchoin L, Pollard TD (1999) *J Biol Chem* 274:15538–15546.
23. Melki R, Fievez S, Carlier MF (1996) *Biochemistry* 35:12038–12045.
24. Vavylonis D, Yang Q, O'Shaughnessy B (2005) *Proc Natl Acad Sci USA* 102:8543–8548.
25. Stukalin EB, Kolomeisky AB (2006) *Biophys J* 90:2673–2685.
26. Weber A, Pennise CR, Fowler VM (1999) *J Biol Chem* 274:34637–34645.
27. Pantaloni D, Hill TL, Carlier MF, Korn ED (1985) *Proc Natl Acad Sci USA* 82:7207–7211.
28. Coue M, Korn ED (1986) *J Biol Chem* 261:1588–1593.
29. Weber A, Northrop J, Bishop MF, Ferrone FA, Mooseker MS (1987) *Biochemistry* 26:2537–2544.
30. Carlier MF, Criquet P, Pantaloni D, Korn ED (1986) *J Biol Chem* 261:2041–2050.
31. Pollard TD, Borisy GG (2003) *Cell* 112:453–465.
32. Burt CT, Glonek T, Barany M (1977) *Science* 195:145–149.
33. Maciver SK, Weeds AG (1994) *FEBS Lett* 347:251–256.
34. Spudich JA, Watt S (1971) *J Biol Chem* 246:4866–4871.
35. Pollard TD (1984) *J Cell Biol* 99:769–777.
36. Pollard TD, Goldberg I, Schwarz WH (1992) *J Biol Chem* 267:20339–20345.

SI Text

Depolymerization kinetics of ADP-actin in the presence of P_i

In this section we present the equations that we used to fit the dependence of the rates of ADP-actin dissociation from filament ends on the concentration of phosphate (Fig. 3). For clarity, we use a notation slightly different from the main text. The following analysis applies equally to barbed and pointed ends. We start with the case where the equilibrium dissociation constant for phosphate binding to ADP-actin filaments, $K_{\mathrm{d,fil}}^{\mathrm{Pi}}$, is the same for every subunit in the filament. We allow for the possibility that the rate constants for P_i dissociation and association are different on the terminal subunit, but we assume that the ratio of these rate constants is the same as for interior subunits. In the absence of free actin subunits (and thus the absence of subunit association) but in the presence of P_i the rate of subunit dissociation at steady state, *j*, is given by

$$j = -k_D^-(1-p_P) - k_P^- p_P \text{ , [1]}$$

where k_D^- and k_P^- are the dissociation rate constants for ADP-actin and ADP-P_i-actin, respectively. Here p_P is the probability that the terminal subunit binds phosphate, which satisfies

$$\frac{dp_P}{dt} = k_D^-(1-p_P)\theta_P - k_P^- p_P(1-\theta_P) - r_{\mathrm{Pi,term}}^- p_P + r_{\mathrm{Pi,term}}^+[\mathrm{P_i}](1-p_P) \text{ . [2]}$$

where $\theta_P = [\mathrm{P_i}]/([\mathrm{P_i}] + K_{\mathrm{d,fil}}^{\mathrm{Pi}})$ is the probability that the penultimate subunit binds phosphate and $r_{\mathrm{Pi,term}}^-$ and $r_{\mathrm{Pi,term}}^+ = r_{\mathrm{Pi,term}}^- / K_{\mathrm{d,fil}}^{\mathrm{Pi}}$ are the phosphate dissociation and association rate constants on the terminal ADP-actin subunit. In Eq. **2** we assumed that the binding of phosphate in the interior of the filament has reached equilibrium. Thus following a dissociation event the probability that the terminal subunit is ADP- P_i-actin is

θ_P and the probability that the terminal subunit is ADP-actin is $1-\theta_P$. Setting both sides of Eq. **2** to zero at steady state one obtains

$$p_P = \frac{r^+_{\mathrm{Pi,term}}[\mathrm{P_i}] + k^-_D \theta_P}{r^-_{\mathrm{Pi,term}} + r^+_{Pi,term}[\mathrm{P_i}] + k^-_D \theta_P + k^-_P (1-\theta_P)} \,. \quad [\mathbf{3}]$$

Substituting Eq. **3** into **1** we obtain an expression for *j* in a closed form. SI Fig. 7 compares Eq. **1** with the results of a Monte Carlo simulation of the depolymerization process. Both methods give identical results.

We note that if the dissociation equilibrium constant for phosphate on the terminal subunit, $K^{\mathrm{Pi,term}}_{\mathrm{d,fil}}$, is different from the dissociation equilibrium constant for phosphate on interior subunits, $K^{\mathrm{Pi}}_{\mathrm{d,fil}}$, then actin subunit association and dissociation rate constants depend on the type of neighboring actin subunits (see next section). Eqs. **1**-**3** are still valid, provided that we assume that dissociation rate constants are independent of neighbors, i.e., if we assume that the state of neighboring subunits only influences association rate constants. In this case in Eq. **3** one has $r^+_{\mathrm{Pi,term}} = r^-_{\mathrm{Pi,term}} / K^{\mathrm{Pi,\,term}}_{\mathrm{d,fil}}$.

Different phosphate dissociation equilibrium constants on terminal and interior subunits: constraints on rate constants from detailed balance

From detailed balance, in equilibrium, the net rate of transitions between any pair of states is zero. This condition constrains the values of the association and dissociation rate constants (1). In this section we show that when the equilibrium dissociation constant for phosphate at the terminal subunit is different to the equilibrium dissociation constant in the interior of the filament, one has the following constraints from detailed balance:

$$\frac{k^-_{P|P}}{k^+_{P|P}} K^{\mathrm{Pi}}_{\mathrm{d,mon}} = \frac{k^-_{D|D}}{k^+_{D|D}} K^{\mathrm{Pi}}_{\mathrm{d,fil}} \,,\; \frac{k^-_{P|D}}{k^+_{P|D}} = \frac{k^-_{P|P}}{k^+_{P|P}} \frac{K^{\mathrm{Pi,tern}}_{\mathrm{d,fil}}}{K^{\mathrm{Pi}}_{\mathrm{d,fil}}} \,,\; \frac{k^-_{D|P}}{k^+_{D|P}} = \frac{k^-_{D|D}}{k^+_{D|D}} \frac{K^{\mathrm{Pi}}_{\mathrm{d,fil}}}{K^{\mathrm{Pi,tern}}_{\mathrm{d,fil}}} \,, \; [\mathbf{4}]$$

where $k^-_{D|P}$ is the depolymerization rate constant of ADP-actin, given that the penultimate subunit is ADP-P_i-actin and similarly for the other dissociation and association rate constants. $K^{\mathrm{Pi}}_{\mathrm{d,mon}}$ is the phosphate equilibrium dissociation constant from monomers in the bulk. Eq. **4** is applicable to the rate constants of both ends separately, thus ensuring the absence of treadmilling in the presence of phosphate in equilibrium. The ratios $k^-_{D|D}/k^+_{D|D}$ and $k^-_{P|P}/k^+_{P|P}$ have identical values at the two ends; this ensures that there is no treadmilling in either the absence or in the presence of saturating phosphate concentrations. It can be seen in Eq. **4** that when $K^{\mathrm{Pi,term}}_{\mathrm{d,fil}} \neq K^{\mathrm{Pi}}_{\mathrm{d,fil}}$, the actin association and/or dissociation rate constants are different depending on the type of the neighboring actin subunit.

To derive Eq. **4** we note that at equilibrium the rate of association of ADP-P_i-actin onto an ADP-actin terminal subunit is equal to the rate of dissociation of ADP-P_i-actin off an ADP-actin penultimate subunit:

$$k^+_{P|D}[\mathrm{ADP-P_i-actin}](1-p_p) = k^-_{P|D}\,p_P(1-\theta_P) \quad [\mathbf{5}]$$

where p_P is now the equilibrium probability that the terminal subunit binds phosphate and θ_P is the equilibrium probability that an interior subunit binds phosphate. Similarly one has

$$k^+_{P|P}[\mathrm{ADP-P_i-actin}]p_p = k^-_{P|P}\,p_P\theta_P,$$

$$k^+_{D|D}[\mathrm{ADP-actin}](1-p_p) = k^-_{D|D}(1-p_P)(1-\theta_P),$$

$$k^+_{D|P}[\mathrm{ADP-actin}]p_p = k^-_{D|P}(1-p_P)\theta_P. \quad [\mathbf{6}]$$

Eq. **4** is derived from Eqs. **5** and **6** after using $\theta_P = [\mathrm{P}_i]/([\mathrm{P}_i] + K_{\mathrm{d,fil}}^{\mathrm{Pi}})$, $p_P = [\mathrm{P}_i]/([\mathrm{P}_i] + K_{\mathrm{d,fil}}^{\mathrm{Pi,tern}})$, and $[\mathrm{ADP-P_i-actin}] \times K_{\mathrm{d,mon}}^{\mathrm{Pi}} = [\mathrm{P}_i][\mathrm{ADP-actin}]$.

Detailed balance constraints on ATP-actin rate constants and their influence on the critical concentration of ATP-actin

In the previous section, we neglected reactions involving ATP hydrolysis and synthesis, because the rate of ATP synthesis from ADP and P_i is so slow that no ATP should be synthesized in our experiments with ADP and P_i. The discussion above thus applied to those states involving only ADP-actin and ADP-P_i-actin in equilibrium. However accounting for ATP hydrolysis and synthesis does not modify the constraint of Eq. **4**, because detailed balance applies to any pair of states in equilibrium. To add ATP hydrolysis and synthesis to the possible reactions we denote the equilibrium constants for ATP hydrolysis on ATP-actin monomers, $K_{\mathrm{H,mon}}$, filaments, $K_{\mathrm{H,fil}}$, and terminal filament subunits, $K_{\mathrm{H,fil}}^{\mathrm{term}}$. Then one has the following constraint involving the rate constants for ATP-actin association and dissociation (subscript T):

$$\frac{k_{T|T}^-}{k_{T|T}^+} K_{\mathrm{H,mon}} = \frac{k_{D|D}^-}{k_{D|D}^+} K_{\mathrm{H,fil}}\,,\ \frac{k_{T|D}^-}{k_{T|D}^+} = \frac{k_{T|T}^-}{k_{T|T}^+} \frac{K_{\mathrm{H,fil}}^{\mathrm{tern}}}{K_{\mathrm{H,fil}}}\,,\ \frac{k_{D|T}^-}{k_{D|T}^+} = \frac{k_{D|D}^-}{k_{D|D}^+} \frac{K_{\mathrm{H,fil}}}{K_{\mathrm{H,fil}}^{\mathrm{tern}}}\,. \quad [7]$$

Eq. **7** applies separately to the barbed and pointed ends and the ratio $k_{T|T}^- / k_{T|T}^+$ has identical values at both ends to prevent treadmilling of all-ATP-actin filaments.

The values of $K_{\mathrm{H,fil}}$ and $K_{\mathrm{H,fil}}^{\mathrm{term}}$ are not known. For the pointed end we argue in the main text that $K_{\mathrm{d,fil}}^{\mathrm{Pi,term}} > K_{\mathrm{d,fil}}^{\mathrm{Pi}}$. This leads us to expect that $K_{\mathrm{H,fil}}^{\mathrm{term}} > K_{\mathrm{H,fil}}$ for the pointed end. From Eq. **7** this implies that $k_{T|D}^- / k_{T|D}^+ > k_{T|T}^- / k_{T|T}^+$. This inequality is consistent with the curves of Fig. 5*B* where we assumed that $k_{T|D}^+ < k_{T|T}^+$ and $k_{T|D}^- = k_{T|T}^-$.

In Fig. 5*B* we have chosen to modify $k^+_{T|D}$ instead of $k^-_{T|D}$ but we note that the value of $k^-_{T|D}$ is also important, because it influences the elongation rate, although to a lesser extent than $k^+_{T|D}$ (compare Fig. 5*B* and SI Fig. 8*A*). This observation suggests that the critical concentration is higher at the pointed end than the barbed end mostly because of cooperative effects involving the association of ATP-actin rather than the dissociation step. Assuming fast P_i dissociation from the terminal subunit, the value of the rate constant for association of ATP-actin onto a terminal ADP-actin subunit $k^+_{T|D}$ has a much larger influence on the pointed end critical concentration of ATP-actin than the rate constant for association of ATP-actin onto a terminal ADP-Pi-actin subunit $k^+_{T|P}$ (SI Fig. 8*B*). For the same reason, cooperative effects in the dissociation rate constant of ADP-Pi-actin also have a small effect (SI Fig. 8*C*). We note that the dependence of the critical concentration at the pointed end on $k^+_{T|D}$ depends on the rate of ATP hydrolysis by the terminal subunit, which may differ to the rate of ATP hydrolysis by interior subunits (SI Fig. 8*D*).

Parameters of fits in Fig. 3

In Fig. 3*A* we fitted the data to Eq. **1**, using KaleidaGraph 3.51 (Synergy software, Reading, PA). The parameters are as follows. For the continuous line we assumed $r^-_{\mathrm{Pi,term}}$ = 0.003 s^{-1} and obtained the following parameter values: $K^{\mathrm{Pi}}_{\mathrm{d,fil}}$ = 48 mM, k^-_D = 5.3 s^{-1}, k^-_P = 0.12 s^{-1}. For the dashed line we assumed $r^-_{\mathrm{Pi,term}}$ = 20 s^{-1} and obtained the following parameter values: $K^{\mathrm{Pi}}_{\mathrm{d,fil}}$ = 1.2 mM, k^-_D = 5.3 s^{-1}, k^-_P = 0.1 s^{-1}. For the dotted line we assumed $r^-_{\mathrm{Pi,term}}$ = 0.003 s^{-1}, $K^{\mathrm{Pi}}_{\mathrm{d,fil}}$ = 1.5 mM, k^-_P = 0.13 s^{-1} and the fit gave k^-_D = 5.5 s^{-1}.

Similarly, in Fig. 3*B* the parameters were as follows. For the continuous line we assumed $r^-_{\mathrm{Pi,term}}$ = 0.003 s^{-1} and obtained: $K^{\mathrm{Pi}}_{\mathrm{d,fil}}$ = 61 mM, k^-_D = 0.24 s^{-1}, k^-_P = 0.02 s^{-1}. For the dashed line we assumed $r^-_{\mathrm{Pi,term}}$ = 20 s^{-1} and obtained: $K^{\mathrm{Pi}}_{\mathrm{d,fil}}$ = 6.2 mM, k^-_D = 0.24 s^{-1}, k^-_P

= 0.02 s^{-1}. For the dotted line we assumed $r^-_{\mathrm{Pi,term}} = 0.003\ s^{-1}$, $K^{\mathrm{Pi}}_{\mathrm{d,fil}} = 1.5$ mM, $k^-_P = 0.02\ s^{-1}$ and the fit gave $k^-_D = 0.29\ s^{-1}$. The gray line is a fit, using Eq. **2** in which we assumed $r^-_{Pi,term} = 20\ s^{-1}$, $K^{\mathrm{Pi}}_{\mathrm{d,fil}} = 1.5$ mM, $k^-_{D|P} = k^-_{D|D}$, $k^-_{P|P} = k^-_{P|D}$; the fit gave $K^{\mathrm{Pi,term}}_{\mathrm{d,fil}} = 6.3$ mM, $k^-_{D|P} = 0.24\ s^{-1}$, and $k^-_{P|P} = 0.02\ s^{-1}$. We note that the assumptions $k^-_{D|P} = k^-_{D|D}$, $k^-_{P|P} = k^-_{P|D}$ imply constraints on the association rate constants through Eq. **4**. However these association rate constants are irrelevant in the depolymerization data of Fig. 3.

Monte Carlo simulations of polymerization and depolymerization kinetics

We used a kinetic Monte Carlo method (2) to evaluate elongation rates in cases where we could not obtain an analytical expression. We tested the validity of the Monte Carlo method in SI Fig. 7. This method was used to calculate the elongation rates in Figs. 4*B* and 5*B*.

We also used the Monte Carlo method to fit the dependence of the elongation rate on phosphate and actin concentrations in Fig. 2 *B* and *E* (curves not shown). We neglected cooperative affects by assuming that all rate constants are independent of the nucleotide bound to neighboring actin subunits at filament ends. In the simulation the ADP-actin polymerization rate constants were taken from the first rows of Table 1. The association rate constant for P_i binding to the sides of actin filaments was determined from detailed balance (see main text), leaving as the only free parameter in the fit the equilibrium dissociation constant for P_i binding to actin monomers. The optimal value was determined by a global least squares fit to the data of 2, 3, and 4 μM actin (Fig. 2 *B* and *E*) and using only the data for positive elongation rates. In the fit we did not include the experiments for 1 μM actin, which were performed separately and thus deviated slightly from the global trend.

1. Hill TL (1987) *Linear aggregation theory in cell biology.* (Springer: New York).

2. Vavylonis D, Yang Q, O'Shaughnessy B (2005) *Proc Natl Acad Sci USA* 102:8543-8548.